Proceedings Paper:
Hussain, S, Hunter, T orcid.org/0000-0003-3922-491X, Peakall, J et al. (2 more authors) (2022) Remote Analysis of Complex Mineral Suspensions in Engineered Pipelines: Utilizing Underwater Acoustic Backscatter Systems – 22142. In: WM Symposia Conference Proceedings. Waste Management Symposium, 06-10 Mar 2022, Phoenix, Arizona, USA. WM Symposia .

Remote Analysis of Complex Mineral Suspensions in Engineered Pipelines: Utilizing Underwater Acoustic Backscatter Systems – 22142

Serish Tanya Hussain *, Timothy Hunter *, Jeff Peakall **, Hugh Rice*** and Martyn Barnes ****
* University of Leeds, School of Chemical and Process Engineering, Leeds, UK
** University of Leeds, School of Earth and Environment, Leeds, UK
***University of Leeds, School of Mechanical Engineering, Leeds, UK
**** Sellafield Ltd, Warrington, UK

ABSTRACT

Two nuclear waste simulants were used in this paper; aqueous suspensions of magnesium hydroxide and calcium carbonate which were suspended in an engineered pipeline. The physical and flow properties of the suspensions were analyzed online using a commercial ultrasonic velocity profiler (UVP) in backscatter mode. Bespoke probe holders were situated both on horizontal and vertical sections of pipe, where transducers were mounted remotely and held flush to ensure a secure connection to the outside of the pipe. A transducer of 4 MHz frequency (with a 2.5 mm active radii) was mounted onto each probe holder at 90° to the flow, two transducers were used throughout this paper. The two transducers mounted in each probe holder were used to produce concentration data from the slurries using the raw echo amplitude output from the acoustic backscatter system. Various flow regimes were initially tested to understand particle deposition within the pipe. The flow rate within the pipe was maximized to ensure the bulk flow was suspended and to confirm the accuracy of the expected velocity profiles within turbulent flow. Acoustic profiles were then produced by taking the logarithmic translation of the voltage. The voltage values were calculated using the raw echo amplitude measurements from the acoustic backscatter system across a 63 second time period. The concentration of sediment in the pipe loop was varied, and measurements were taken across a concentration array for both nuclear waste simulants. The resulting acoustic profiles were used to extract acoustic attenuation coefficient values. The attenuation coefficients were extracted as a linear function of the gradient between the plot of logarithmic function with distance. Attenuation coefficients are used as a calibration technique as they can be directly compared to coefficients derived from previous literature. This simple calibration procedure allows the UVP (ultrasonic velocity profiler) to directly measure concentration changes of the slurries during pumping. The resulting attenuation coefficient values can be used to extract particle size information using analytical acoustic models. Data collected from vertical pipe arrangements were found to provide sedimentation attenuation coefficients more accurate to calibration data from previous literature. The slurry suspensions running through the horizontal pipe arrangements were more prone to segregation in the pipe.

Overall, this project provided critical information into concentration variation of the nuclear slurries with flow, while also allowing examination of the role of shear on fluctuations in mean particle-aggregate sizes. This understanding is vital for ongoing nuclear waste processing, to ensure accurate accounting of the radioactive sludges during transfer. Knowledge of concentration variation in pipe flow will help establish physical changes that may impact downstream processing in post-interim storage. As data were collected in real-time and remotely, the safety of workers was not compromised. The whole system can be mounted remotely without contact with the nuclear waste suspension. This online characterization technique can be applied to complex suspensions in many industries which would help in cutting down costs and improving analysis time. Remote techniques are becoming more popular, especially in this global climate, as a way to protect workers and decrease the possibility of contamination and are ideal because no *ex-situ* measurements are taken, samples are not required and there is no preparation needed for the suspension.

INTRODUCTION

Complex suspensions exist across all industries, whether it be nuclear waste slurries and sludges, wastewater streams, emulsions in food and personal care products, and so forth. Complex systems are difficult to characterize, especially in sectors like nuclear, where extracting samples for analysis is too hazardous to conduct routinely [1]. A particular focus in the nuclear waste sector within the U.K, is the characterization of Magnox storage ponds at Sellafield, which contain corroded magnesium hydroxide sludge. The current plan for these complex wastes is transportation in engineered pipelines to a safe containment facility for long-term storage. This storage is an interim step before ultimate encapsulation and disposal [2]. These Magnox suspensions have been left in their current open storage ponds for many decades where foreign materials have been introduced from the open-air environment. Therefore, it is imperative that the wastes are characterized before or during transportation [3]. To this end, this paper focuses on the remote, physical characterization of nuclear waste simulant slurries during transportation via the application of an acoustic backscatter system (ABS), using a commercial ultrasonic velocity profiler (UVP). The UVP is predominantly used to extract velocity profiles, however, for this paper the system has been utilized to extract echo amplitude values for acoustic profiling, which can be used to understand the scattering-attenuating properties of suspensions [4][5]. Attenuation is dependent on particle size, density, and concentration. Therefore, differing nuclear waste simulants should provide more insight into the effect of particle size and concentration on attenuation through an engineered pipeline [6]. The UVP is compatible with transducers with frequencies of 0.5, 1, 2, 4 and 8 MHz, where it allows the connection of multiple probes to produce simultaneous data from different locations along the pipeline, for example. Ultrasonic transducers utilized with the UVP also have a range of active radii from 2.5 and 5 mm. However, for transducers to be mounted flush against a standard 1-inch pipe, a small active radius is required, therefore probes with 2.5 mm active radii were utilized [7]. In this paper, two nuclear waste simulants were used: calcium carbonate (calcite) and commercial magnesium hydroxide powder. Calcite ($CaCO_3$) is a crystal form of calcium carbonate that has been used in previous literature as a nuclear waste simulant, while the magnesium hydroxide is more chemically similar to the Magnox sludge in the Sellafield storage ponds [8][9][10]. Simulant waste suspensions were analyzed in an engineered pipeline in both horizontal and vertical arrangements to produce acoustic profiles, where sedimentation attenuation coefficients were extracted from the acoustic profiles and compared to coefficients calculated from calibration data. From direct comparison of coefficients, the pipeline arrangement which was determined to give a more accurate attenuation coefficient value was selected as the pipeline arrangement for ongoing monitoring and analysis [9]. As magnesium hydroxide has not been used in previous literature to produce calibration data, results were compared to estimations of the viscous attenuation calculated using established theory for fine suspensions in the Rayleigh regime.

THEORY

The raw data directly produced from the UVP is in the form of raw echo values. This raw echo data can be directly converted to the root mean square voltage. For conversion of the raw echo data, the amplification of the sound signal needs to be known. A compromise value for gain is selected throughout the experiments to allow the sound signal to be amplified consistently. High gain values may produce an artificial sound signal and increase system noise, whereas, if the gain value is too low then the amplification of the sound signal is not strong enough for signal detection [5]. A compromise gain value was chosen and used to convert the raw echo values to root mean square voltages, as shown in Eq. (1) [11].

$$V(r) = \frac{3.052\ x\ 10^{-4} E(r)}{g(r)} \tag{1}$$

Once the voltage values have been calculated, the factors which effect the voltage can be investigated. Voltage is a function of the sediment backscatter constant (k_s in m.kg$^{0.5}$), the transducer constant (k_t in

$V.m^{1.5}$), the near field correction factor (ψ), distance from the transducer (r in m), particle concentration (M in $kg.m^{-3}$), attenuation due to solid (α_s in m^{-1}) and attenuation due to water (α_w in m^{-1}), this is shown in Eq. (2) [5].

$$V = \frac{k_s k_t}{\psi r} M^{1/2} e^{-2r(\alpha_w + \alpha_s)} \tag{2}$$

The near field correction factor is calculated using the distance from the transducer (r in m), active radius (a_t in m) and wavelength of transducer (λ in m); where wavelength is the speed of sound over frequency (4 MHz) (Eq. (3)) [11][12]. It is used in this paper to counteract the complex near field acoustic behavior and encourage a linear profile in the near field region. The speed of sound can be assumed to be that in water (1480 m/s) due to the low concentrations of simulants used in this paper, however, it has been found that aqueous suspensions of sufficient density will start to alter the speed of sound [13][14]. Therefore, the Urick equation was used to calculate the expected speed of sound in sediment suspensions of magnesium hydroxide and calcite.

$$\psi = \frac{1 + 1.35\left(\frac{r}{\pi a_t^2/\lambda}\right) + \left(2.5\left(\frac{r}{\frac{\pi a_t^2}{\lambda}}\right)\right)^{3.2}}{1.35\left(\frac{r}{\pi a_t^2/\lambda}\right) + \left(2.5\left(\frac{r}{\frac{\pi a_t^2}{\lambda}}\right)\right)^{3.2}} \tag{3}$$

The speed of sound in the sediment suspensions is calculated using Eq. (4), where the speed of sound is a function of the density (ρ in $kg.m^{-3}$) and compressibility (k in $m^2.N^{-1}$) of the suspension.

$$c = \frac{1}{\sqrt{\rho k}} \tag{4}$$

The density and compressibility are expressed as additive properties of their corresponding quantities in previous literature. Hence, Eq. (5) and (6) are used to calculate the additive properties for both density and compressibility; in Eq. (5) and (6), ϕ indicates the concentration by volume of the sediment whilst the subscript w and s indicate values for water and solid, respectively.

$$\rho = \rho_w \phi + \rho_s (1 - \phi) \tag{5}$$

$$k = k_w \phi + k_s (1 - \phi) \tag{6}$$

A value for the compressibility of water from previous literature was used in Eq. (6) ($k_w = 4.578.10^{-10}$ $m^2.N^{-1}$ [15]). The bulk moduli of calcite (77.10^9 Pa) and magnesium hydroxide ($43.3.10^9$ Pa) were extracted from previous literature [16][17]. The compressibility (k in $m^2.N^{-1}$) of both particle species were calculated by taking the inverse of the bulk moduli ($k_{s\text{-}Mg(OH)2} = 2.31^{-11}$ $m^2.N^{-1}$, $k_{s\text{-}calcite} = 1.30.10^{-11}$ $m^2.N^{-1}$). The overall density and compressibility values for the suspension are calculated by inputting all compressibility and density values into Eq. (5) and Eq. (6). These density and compressibility values are used in Eq. (4) to determine the overall speed of sound. The speed of sound for the highest concentration (35.71 g/L) of calcite suspension was estimated from these correlations to be 1473 m/s, which is slower than the speed of sound through water. The speed of sound for magnesium hydroxide at the highest solid suspension concentration (35.71 g/L) was calculated to be 1476 m/s, also slower than the speed of sound through water, although for both species the difference is less than 1%. Therefore, as the speed of sound is only used to calculate the near-field region in Eq. (3), to simplify calculations, the speed of sound through water was used in Eq. (3).

All calculated variables and constants through Eq. (1) to (3) can be used to calculate the *G*-function which is a logarithmic form of the voltage function. The *G*-function is derived using the voltage (*V* in volts), near field correction factor (ψ, dimensionless) and distance from the transducer (*r* in m) [11].

$$G = \ln(\psi r V) = \ln(k_s k_t) + 0.5\ln(M) - 2r(\alpha_w + \alpha_s) \tag{7}$$

The sedimentation attenuation coefficient (ξ_s in $m^2.kg^{-1}$) can be calculated by using the double differentiation of *G*. The attenuation coefficient is calculated for calibration of the experiment [11].

$$\xi_s = -0.5\left(\frac{\partial^2 G}{\partial M \partial r}\right) = -0.5\frac{\partial}{\partial M}\left[\frac{\partial}{\partial r} ln(\psi r V)\right] \tag{8}$$

The normalized scattering cross section (χ) can be calculated from the heuristic expression from Betteridge *et al*. [18]. The normalized scattering value (χ) is a function of the angular wavenumber (*k* in m^{-1}) and particle radius (*a* in m) [18].

$$\chi = \frac{\left[0.24\left(1-0.4e^{\frac{5.5-ka}{2.5^2}}\right)(ka)^4\right]}{[0.7+0.3(ka)+2.1(ka)^2-0.7(ka)^3+0.3(ka)^4]} \tag{9}$$

$$\chi = \xi_s \frac{4a\rho_s}{3} \tag{10}$$

The estimated attenuation coefficients derived using Eq. (4) only account for scattering losses. For systems within the Rayleigh regime, where $ka<1$, viscous losses occur and have to be taken account of. The *ka* values calculated for calcite and magnesium hydroxide are 0.0604 and 0.0419, so both particulate systems are within the Rayleigh regime [19][20]. Viscous losses must be considered for accurate calculation of normalized scattering cross section values. To do this, theoretical models developed by Urick [14] have been used to calculate the viscous attenuation loss for mono-sized spheres. Non-dimensional intermediate variables, β, *t* and θ in Eq. (11) are all used to calculate ξ_{sv}, where *sv* denotes viscous losses. The angular frequency is denoted by ω ($2\pi f$) where *f* is the frequency of the transducer in Hertz (4,000,000) and υ is the kinematic viscosity of water (10^{-6} $m^2.s^{-1}$). The intermediate variables, β, *t* and θ are used to calculate ξ_{sv} in Eq. (12) where β, *t* and θ depend on the density of the particulate (ρ_s $kg.m^{-3}$) used and the density of water (ρ_w $kg.m^{-3}$). The overall attenuation coefficient ($\xi = \xi_s + \xi_{sv}$) is a summation of both the attenuation due to scattering (ξ_s) and attenuation due to viscous losses (ξ_{sv}).

$$\beta = \sqrt{\frac{\omega}{2v}}, \qquad t = \frac{9}{4a\beta}.\left(1+\frac{1}{a\beta}\right), \qquad \theta = 0.5 + \frac{9}{4a\beta} \tag{11}$$

$$\xi_{sv} = \frac{k}{2\rho_s}\left(\frac{\rho_s}{\rho_w}-1\right)^2 \frac{t}{t+\left(\frac{\rho_s}{\rho_w}+\theta\right)^2} \tag{12}$$

EXPERIMENTAL METHODS

Materials

Calcite (Omyacarb 2, Omya AG) is a crystal form of calcium carbonate which is manufactured as a fine white powder and is easily dispersed into aqueous suspensions [20]. Similar material has been used in previous literature as a nuclear simulant [9]. Secondarily, a commercial magnesium hydroxide powder (Versamag Martin Marietta Magnesia Specialties) was also used, which was predicted to have similar fine particle sizes [10][19]. Both nuclear waste simulants are a fine white powder which fully disperse within aqueous suspensions.

The particle size distributions of both calcite and magnesium hydroxide were investigated using a Mastersizer 3000 (Malvern Panalytical) which uses laser diffraction to measure the intensity of light scatter as the laser passes through a dispersed particulate sample. The scattering pattern is analyzed to calculate the size of the particles [21][11]. The cumulative particle size distributions for both species are shown in Fig. 1. The particle size distributions for both calcite and magnesium hydroxide exhibit approximately bimodal distributions, which shows that there are a couple of particle size groups. The smaller peak shown at approximately 0.8 µm for the calcite system can be attributed to fines within the suspension likely generated from production milling. However, all calcite particles possess a fairly small particle size range of less than 13 µm and more than 0.1 µm, with 80% being between 1-13 µm. The magnesium hydroxide also shows a broader bimodal distribution, which in this case is attributed to aggregate build-up within the suspension. The d50 for both calcite and the magnesium hydroxide were calculated using Fig. 1. Corresponding particle size for 50% volume shows the particle size where 50% of the suspension exists. This is correlated to the d50 of the suspension. The specific d50 extracted for calcite and magnesium hydroxide are 4.5 and 13 µm, respectively. The difference in particle size is due to the increased existence of larger aggregates in the magnesium hydroxide and the existence of fines in calcite.

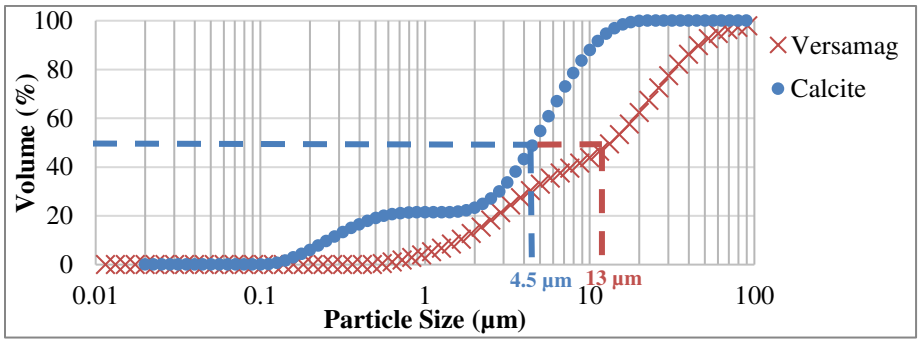

Fig. 1. Cumulative particle size distributions of calcite and magnesium hydroxide.

Fig. 1 shows that both materials are complex fine particulates which require complex analysis. Therefore, a desktop scanning electron microscope (TM3030Plus SEM, Hitachi) was used to produce micrographs of calcite and the magnesium hydroxide powders. Fig. 2a and b show the micrographs for calcite. The calcite shows a varied particle size distribution with a complicated structure in Fig. 2, where fines of less than 2 µm can be seen across the micrograph. It is difficult to distinguish individual particles as the calcite crystals are packed together, and the size range is at the limit of resolution of the desktop SEM. Fig. 3a and b show the SEM images taken when analyzing the magnesium hydroxide.

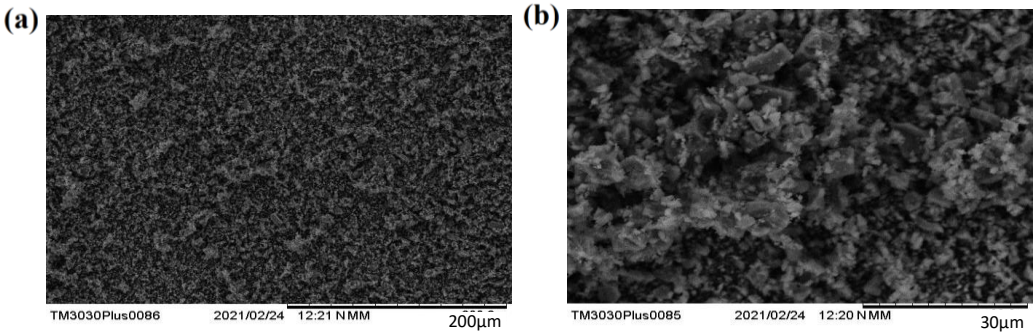

Fig. 2. SEM images of calcite powder.

From Fig. 3a and b, the magnesium hydroxide shows a varied particle size distribution, much like the calcite. Larger aggregates can be seen in Fig. 3a and b which show the increased d50 of magnesium hydroxide shown in Fig. 1. Finer particles are shown as well but the desktop SEM is unable to clearly distinguish between the individual particles. The range of aggregate sizes is what leads to an increased d50 in Fig. 1. [22]

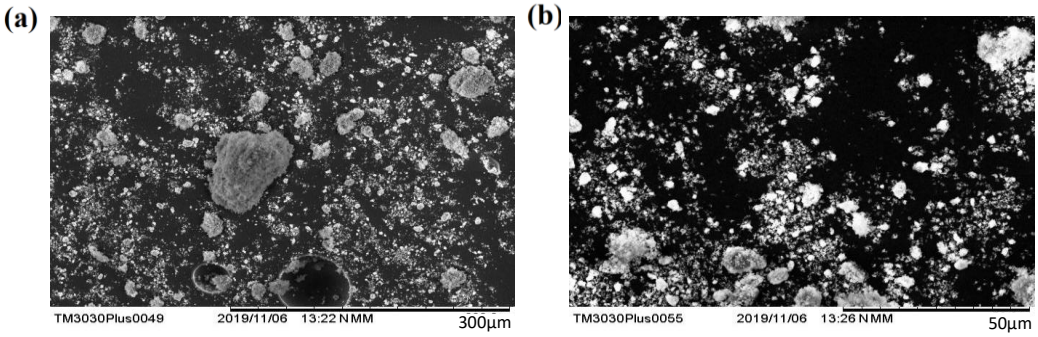

Fig. 3. SEM images of magnesium hydroxide powder.

Pipeline

A pipeline was built and erected onto stainless steel struts to ensure stability of the loop. A schematic of the engineered pipeline is shown in Fig. 4. The pipes are annotated with dimensions to provide a sense of the scale. The pipe loop was constructed using uPVC (unplasticized polyvinyl chloride) sections of pipe, where the outer and inner diameters of the pipe were 30 and 25 mm, respectively [23]. The green arrows show the direction of flow so readers can easily track the movement of suspension. The yellow triangles indicate the location of a valve. Two-way valves are shown by two triangles facing each other whilst three-way valves are shown by three triangles. The black boxes show the location of probe holders. One probe holder was mounted onto a vertical section of pipe and another on a horizontal pipe section. An ultrasonic transducer was mounted at each probe location which allowed analysis of the suspension in a horizontal and vertical pipe section. The bespoke probe holders were manufactured to allow transducers to be slotted in and held flush against the surface of the pipe. The pipe loop was set at a flow rate of 0.53 L/s to ensure that the suspension was fully dispersed within the pipe.

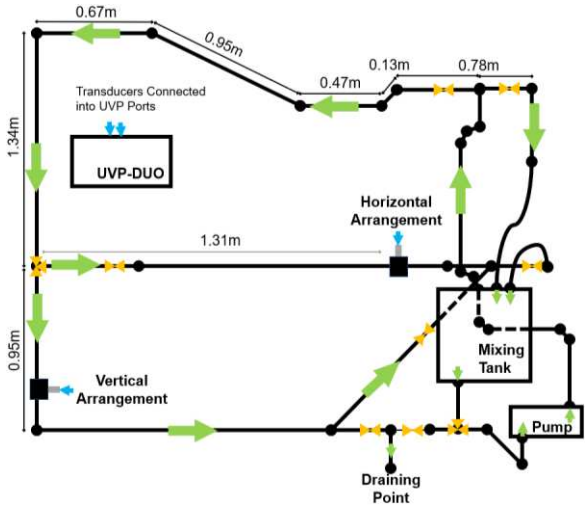

Fig. 4. Engineered pipeline with dimensions and flow direction.

The bulk suspension ran through each pipe section to allow accurate analysis of the suspension in the two pipe sections. The top half of the pipe loop was isolated for analysis of the suspension through the horizontal section of pipe. This ensured that the bulk suspension flowed through the probe holder on the horizontal pipe. The isolation of the top half of the pipe was achieved by using the three-way valve on the left of the horizontal pipe. The same three-way valve was used to shut off the horizontal pipe section and run the bulk suspension through the vertical pipe section. This allowed analysis of the suspension through the vertical probe holder. In this way, by isolating each section, the bulk suspension flowed through each arrangement. The pipe length underneath the mixing tank was used for draining the suspension. The sediment suspensions were drained for waste disposal once all experiments had concluded. Water was circulated in the pipe loop to clean the pipe loop and remove any material which had settled in the pipe [10]. The transducers were mounted at 90° to the flow and were used to gather sound attenuation data across the pipe. The probes were connected to the UVP in frequency dependent slots [7]. As the pipe arrangements were isolated one at a time, the transducers cannot be used simultaneously; instead, they were used consecutively.

The transducers must be mounted onto the pipe and held flush against the pipe. Due to the curvature of the pipe this can be difficult to do. The pipe can be shaved down to produce a flat edge, but the pipe walls are too thin. Any shaving of the pipe would risk causing cracks and leaks in the pipe loop [24]. An audio jelly layer is placed between the transducer and pipe wall to assist with the sound penetration through the pipe wall. The transducers send out a sound signal over a time period of 62 ms for 1023 profiles. This resulted in a total measurement time of 63 seconds for each suspension concentration analyzed [7]. Varying concentrations of calcite were suspended in the mixing tank, with the mixer-impeller system at a steady rate of 800 rpm. This high rotation rate ensured the calcite dispersed homogeneously through the tank. The mixer-impeller system ran for approximately a minute before the pump was turned on and the suspension travelled through the pipe loop. The pump moved the suspension around the pipe loop at a flowrate of 0.53 L/s. The pump ran for approximately 5 minutes before the suspension was analyzed using the ultrasonic transducers. The time delay between turning the pumps on and analyzing the suspension ensured the suspension was homogeneous throughout the pipe loop. The calcite suspension was analyzed at both probe holder positions on the horizontal and vertical pipe sections. Once all concentrations of calcite had been analyzed in both pipe sections, the next step was draining the suspension. The pipe loop was emptied through the drainage point and the experiment was repeated with varying concentrations of magnesium hydroxide.

RESULTS AND DISCUSSION

The acoustic profiles for calcite and magnesium hydroxide were generally displayed as distance dependent *G*-function values, where the *G*-function was calculated with Eq. (7) and was used to understand the effect of sediment type and concentration on attenuation [5][9][11]. For the current study, the *G*-function was plotted against the distance across the pipe diameter and used to extract the sediment attenuation coefficient values for the two different sediment types, which were compared to attenuation coefficient values from calibration data [9].

Calcite

Fig. 5a and b show the acoustic profiles for the calcite suspension travelling through the horizontal pipe arrangement. The start of the suspension environment and the back of the pipe wall spans from 0.006 m to 0.031, which produced an inner diameter of 0.025 m. In the non-contacting arrangement, the sound signal travelled through a thin layer of the probe holder before penetrating the pipe wall, with a thin layer of audio gel between them. The acoustic profile in the first 8 mm is from internal reflections in the probe holder and pipe wall. The UVP expects the signal to travel at the speed of sound in water (1480 m/s), however, the speed of sound through the uPVC solid pipe wall was much faster (2300 m/s). The increased speed of sound through solid was due to the increase in vibrations [25][26]. The faster speed of sound resulted in the signal travelling through the pipe wall quicker than the UVP expected.

The profile was noisy from 0.006 to 0.017 m which was due to near field interference and suspension segregation in the first half of the pipe. Calcite is very dense which explains the noisy profile in the first half of the pipe [20]. The horizontal pipe sections were more likely to encourage segregation which was shown in the non-linear profile from 0.006 to 0.0017 m [27][28]. The end of the pipe was indicated by a dramatic increase in sound signal at 0.031 m. The increase in signal was due to reflections from the back end of the pipe. The inner pipe wall was assumed to be at 0.006 m using the actual inner pipe diameter of 0.025 m and the back end of the pipe [29]. The averaging of the signals across the 63 second measurement time period produces noisy signals, which was shown in all acoustic profiles. However, the likely main reason was that the expected backscatter strength from both sediments is minimal, as they were comprised of fine particulate material that does not scatter significantly. The small proportion of backscatter available for analysis makes it difficult for the UVP to produce a smooth profile. The speed of sound in calcite suspensions was calculated using Urick's equation. The calculated speed of sound was 1473 m/s, which is slightly slower than the speed of sound in water. This should have translated to an increased measured inner diameter; however, the difference in speed of sound was smaller than 1%. Due to the potential complexities from nearfield interference and particle segregation, in-pipe calibration was performed on the horizontal pipe in the lower pipe section from 0.016-0.03 m (with expanded data shown in Fig. 5 (b)). Within this section, the change in G with distance (dG/dr) was approximately linear for each specific concentration, as would be expected for well-mixed suspensions [5] although there was still a large degree of noise associated, as can be evident in Fig. 5 (b). However, the overall averaged attenuation gradients (shown by the dashed lines) do indicate the expected change between concentrations, where higher particle levels lead to greater attenuation and associated dG/dr values [11].

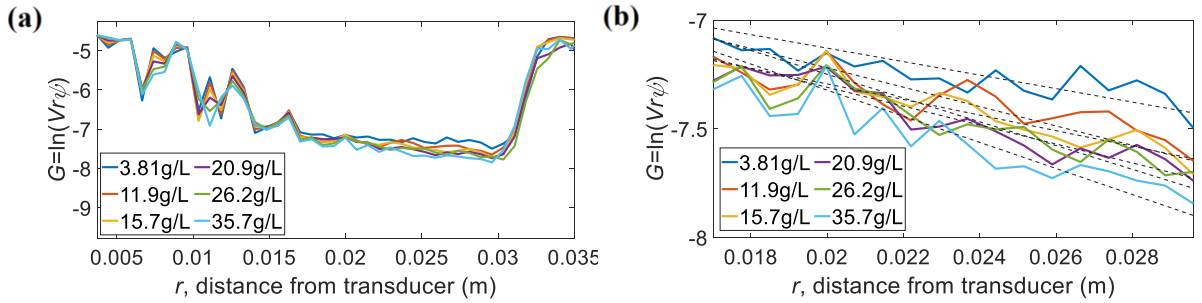

Fig. 5. (a) Acoustic *G*-function profiles from calcite suspensions using the horizontal pipe arrangement and (b) linear region of the acoustic profiles shown in (a) where dashed lines represent linear gradients for each concentration.

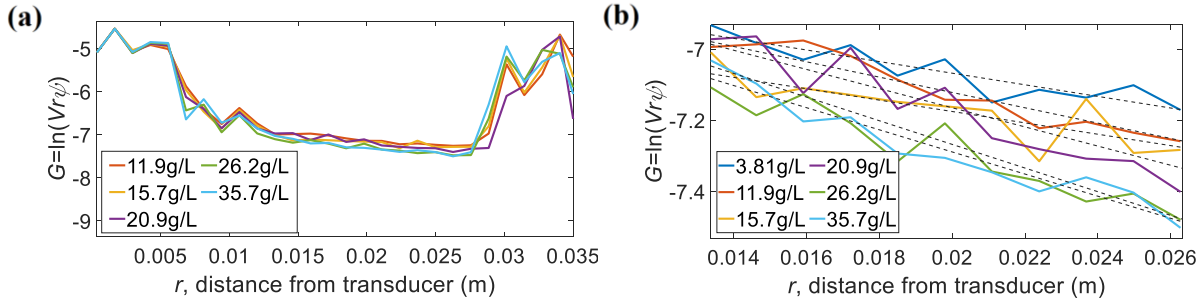

Fig. 6. (a) Acoustic *G*-function profiles from calcite suspensions using the vertical pipe arrangement and (b) linear region of the acoustic profiles shown in (a) where dashed lines represent linear gradients for each concentration.

Fig. 6a shows the acoustic profiles for calcite travelling through the vertical pipe section. The distance required to travel through the pipe wall was the same in the horizontal and vertical acoustic profiles.

Again, the sound signal enters the suspension environment at approximately 0.006 m, where a significant and non-linear reduction in *G* values was observed for the nearfield region from 0.0061 m to 0.012 m, which was the distance closest to the inner pipe wall. The profiles are notably less noisy than the horizontal pipe in this region, inferring that the suspension segregation in the horizontal flow was having additional influence, but the non-linear reduction in *G* was still attributed to acoustic complexities from nearfield interference. Again, the far section of the pipe outside of the immediate nearfield area showed an expected linear reduction in *G* with distance and was used for internal calibration (from 0.014-0.026 m), shown in Fig. 6 (b) where again, the strong sound reflection at 0.0295 m was from the far pipe wall. This showed that the signal entered the suspension at approximately 0.0045 m, this was an approximate value as the speed of sound in the suspension was slower than that in water. The isolation of the linear region further showed that vertical profiles were less noisy than horizontal pipe data. The smoother profile was attributed to limited segregation in the vertical pipe. Acoustic profiles in Fig. 5a and 6a both intercept the y-axis at around -5 which showed that signal strength is similar for both pipe orientations. Similar signal strength indicated that the transducer analyzed calcite suspensions in both pipe sections with similar levels of accuracy [7]. Acoustic profiles in the horizontal pipe appear to attenuate more which could be attributed to the increased effect of particle segregation in the horizontal pipe. Again, average d*G*/d*r* values were taken for each concentration (shown by dashed lines in Fig. 6 (b)) and used to calculate the specific attenuation coefficient.

The speed of sound for varying volume fractions were calculated from the Urick equations. The concentration range used for calcite was converted into a volume fraction and used to calculate the speed of sound; this was shown in Table 1. The particle density of calcite (2711 $kg.m^{-3}$) was used for conversion of mass to volume [20]. Volume % was calculated using the volume of water in the tank (42 L). The compressibility of calcite was calculated using the inverse of the bulk modulus for calcium carbonate [16]. Table 1 shows that an increase in concentration leads to a decrease in speed of sound through the pipe.

TABLE. I Speed of sound calculations for varying volume fractions of calcite

Concentration, *M* ($kg.m^{-3}$)	Mass (kg)	Volume (m^3)	Volume (%)	Density ($kg.m^{-3}$)	Compressibility ($m^2.N^{-1}$)	Speed of sound ($m.s^{-1}$)	Δ*c*/*c0* (%)
3.81	0.16	0.00006	0.15	1000	4.57E-10	1479	-0.041
11.9	0.50	0.00018	0.46	1005	4.56E-10	1478	-0.155
15.7	0.66	0.00024	0.60	1007	4.55E-10	1477	-0.208
20.9	0.88	0.00032	0.80	1011	4.54E-10	1476	-0.279
26.2	1.10	0.00041	1.00	1014	4.53E-10	1475	-0.351
35.7	1.50	0.00055	1.36	1020	4.52E-10	1473	-0.476

Magnesium hydroxide

Fig. 7a and b show the acoustic profiles from magnesium hydroxide suspensions travelling through a horizontal pipe. There was significant noise in the acoustic profile in the first 0.008 m where the signal was disturbed by reflections in the probe holder and pipe wall. The profile was noisy in the first half of the pipe from 0.006 to 0.014 m. The noise was similar to the noise shown in the horizontal profiles using calcite suspensions. Therefore, noise in the first half of the pipe was attributed to near field interference and suspension segregation in the horizontal pipe section. The suspension was analyzed where the profile becomes linear from 0.014 m until 0.032 m, where the signal reflects against the back of the pipe wall. From this reflection point, the inner pipe wall was assumed to be at 0.007 m. This was an approximate distance as the speed of sound in the magnesium hydroxide suspensions was slower than that in water.

The distance between the sound signal entering the suspension environment and signal reflectance against the back wall correlated to the inner pipe diameter.

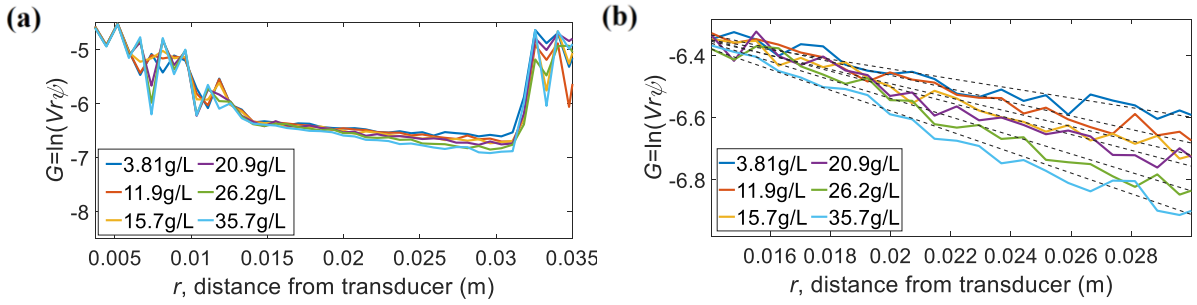

Fig. 7. (a) Acoustic *G*-function profiles from magnesium hydroxide suspensions using the horizontal pipe arrangement and (b) linear region of the acoustic profiles shown in (a) where dashed lines represent linear gradients for each concentration.

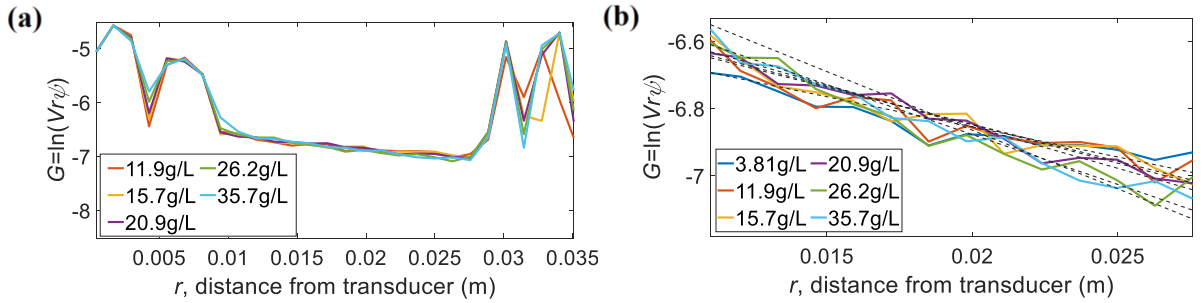

Fig. 8. (a) Acoustic *G*-function profiles from magnesium hydroxide suspensions using the vertical pipe arrangement and (b) linear region of the acoustic profiles shown in (a) where dashed lines represent linear gradients for each concentration.

The speed of sound for magnesium hydroxide suspensions was found in Table 2 where the speed of sound at the highest concentration was slower than the speed of sound in water. The decreased speed of sound travelled through the suspension at a slower rate which leads to an increased measured inner pipe diameter. From Table 2 it is shown that an increase in density caused a decrease in speed of sound. The d50 of magnesium hydroxide extracted from Fig. 1 is 13 µm whereas the d50 for calcite is 4.5 µm. The difference in particle size effected the attenuation of sound through the pipe. The larger particles possess a larger cross-sectional area which leads to an increase in scatter whilst the finer calcite particles have a larger surface area to volume ratio which leads to higher viscous attenuation. This leads to an increase in attenuation for the finer particles. Therefore, the magnesium hydroxide suspensions were expected to attenuate less than the suspensions of calcite. The acoustic profile was segmented to show the isolated linear region in Fig. 7b, where it can be shown that magnesium hydroxide profiles were less noisy than the calcite profiles. The smoother profiles show that the UVP was able to analyze the magnesium hydroxide with more accuracy and efficiency. The acoustic profiles in Fig. 7a intercepts the y-axis at -5 showing that the signal strength for UVP is the same again.

Fig. 8a shows the acoustic profiles extracted from the magnesium hydroxide travelling through the vertical pipe section. The noise in the profiles until 0.008 m was attributed to the near field interference and reflections in the pipe wall. The measured inner pipe diameter was calculated from the point where the signal entered the suspension and ends where the signal reflected. The profiles were linear from 0.009 m to 0.0285 m where the signal reflects against the back pipe wall.

The inner pipe diameter was assumed to be at 0.0035 m by using the inner pipe diameter of 0.025 m and the back of the pipe wall. This was an approximate distance as the speed of sound in magnesium hydroxide suspensions was expected to be slower than the speed of sound in water, this was shown in Table 2. A decreased speed of sound should result in a longer measured distance. Magnesium hydroxide acoustic profiles were expected to attenuate less than calcite due to the increased scattering of magnesium hydroxide. This was shown in Fig. 7b where the profiles were very close together with little difference between varying concentration profiles. The increase in concentration led to an increase in attenuation from the higher density of particles in the suspension. The calculations for the speed of sound in calcite were recreated for the magnesium hydroxide suspensions. The density of magnesium hydroxide used in calculations was 2340 $kg.m^{-3}$[19]. The compressibility for magnesium hydroxide was calculated using the inverse of the bulk modulus of brucite, which is the main crystalline form of magnesium hydroxide mineral [17].

TABLE. II Speed of sound calculations for varying volume fractions of magnesium hydroxide suspensions

Concentration, M ($kg.m^{-3}$)	Mass (kg)	Volume (m^3)	Volume (%)	Density ($kg.m^{-3}$)	Compressibility ($m^2.N^{-1}$)	Speed of sound ($m.s^{-1}$)	$\Delta c/c0$ (%)
3.81	0.16	0.00007	0.17	999	4.57E-10	1480	-0.019
11.9	0.50	0.00021	0.53	1004	4.55E-10	1479	-0.089
15.7	0.66	0.00028	0.70	1006	4.55E-10	1478	-0.121
20.9	0.88	0.00038	0.93	1009	4.54E-10	1478	-0.164
26.2	1.10	0.00047	1.16	1013	4.53E-10	1477	-0.207
35.7	1.50	0.00064	1.58	1018	4.51E-10	1476	-0.282

The speed of sound in magnesium hydroxide suspensions decreases with increasing concentration, much like the calcite suspensions. The speed of sound at the highest concentration of magnesium hydroxide was slower than the speed of sound in water. The main distinction between the calcite and magnesium hydroxide calculations was the speed of sound. The speed of sound in magnesium hydroxide suspensions was slightly higher. This difference in speed of sound was mainly attributed to the difference in density. The change in speed of sound in relation to the speed of sound in water was shown in the last column in Table 1 and 2. [30]. In previous literature, the change in speed of sound for a 3% volume of silica glass beads is -0.75%. When extrapolating, the change in speed of sound values using Table 1 for a 3% volume was -1%, which can be directly compared as the density of calcite is higher than the density of silica glass beads [31].

Comparison of attenuation coefficients

The isolated linear regions of the acoustic profiles were used to extract the sedimentation attenuation coefficient. The gradient of all acoustic profiles shown in Fig. 5b, 6b, 7b and 8b were extracted and plotted versus concentration to produce an overall attenuation profile, shown for both calcite and magnesium hydroxide suspensions in both pipe configurations in Fig. 9a and b, respectively. An increased gradient value in these profiles indicates an increase in attenuation, where the overall attenuation coefficient is -½ of the gradient value (see Eq. (8)).

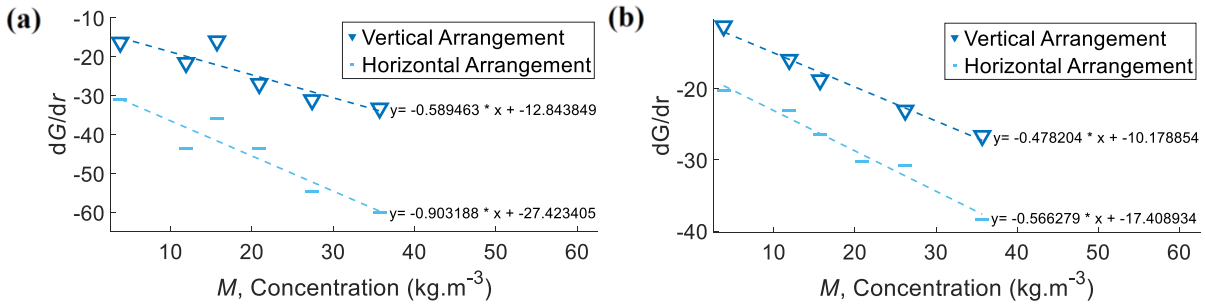

Fig. 9 Attenuation profiles for horizontal and vertical pipe arrangements using suspensions of (a) calcite and (b) magnesium hydroxide.

The suspensions travelling through the horizontal pipe sections all intercept the y axis at a lower value, which shows that particle segregation in the horizontal pipe causes a weaker profile formation. It is evident in both calcite and magnesium hydroxide systems that, as well as having stronger backscatter (larger dG/dr values), the vertical pipe arrangement led to lower overall attenuation (less negative gradient with concentration). This is most likely due to the segregation in the horizontal arrangement, where the average concentration in the lower half of the pipe (where the correlation is taken from) is higher than the expected mean, leading to higher levels of attenuation. As stated, the specific sedimentation attenuation coefficients can be extracted from Fig. 9 by multiplying the gradient by -0.5 (as shown in Eq. (8)) and the measured values are shown in Fig. 10 for both sediment type and pipe sections, with an additional calibration value for the same calcite powder in well mixed conditions taken from previous work by the current authors [5]. The error bars in Fig. 10 are calculated by using the time averaged voltage data over the 1023 profiles. The G-function values can be calculated from the full array of voltage data across the 1023 profiles. A minimum and maximum attenuation coefficient can be extracted by plotting the minimum and maximum G-function values at initial and final distance points.

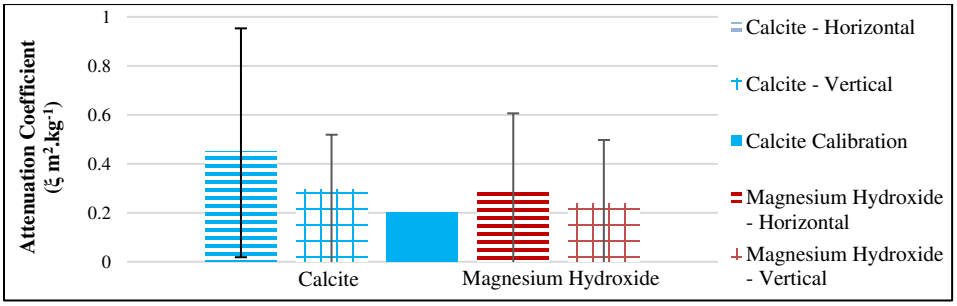

Fig. 10. Attenuation coefficients for calcite and magnesium hydroxide using vertical and horizontal pipe arrangements. Calibration value for calcite taken from literature using a well-mixed impeller tank [5].

The attenuation coefficients from horizontal pipe sections were higher than the attenuation coefficients extracted from the vertical pipe sections, because of the particle segregation in the horizontal pipe leading to an increase in concentration in the measurement zone, as discussed. Interestingly, the attenuation coefficients extracted from calcite suspensions were compared directly to well mixed values from previous literature, where coefficients from the vertical pipe section were closest to the calibration coefficient, inferring that the homogenous mixing of the vertical arrangement leads to more consistent acoustic scattering. It would be proposed therefore that any monitoring of industrial slurry pipelines should use vertical sections for instrument mounts. The degree of variation (shown by the error bars) in the horizontal pipe sections were also larger than from the vertical pipe sections.

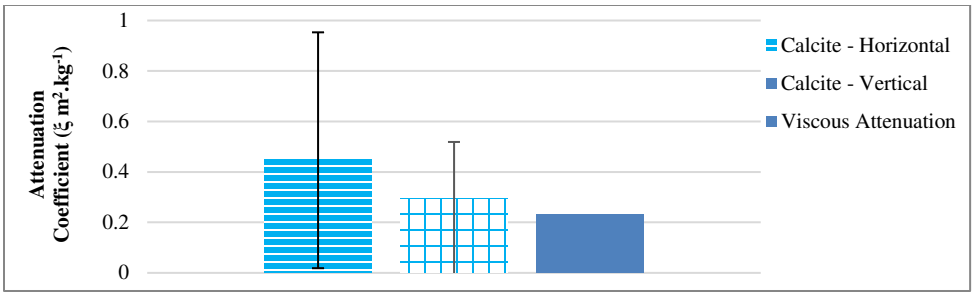

Fig. 11. Viscous attenuation coefficients for suspensions of calcite

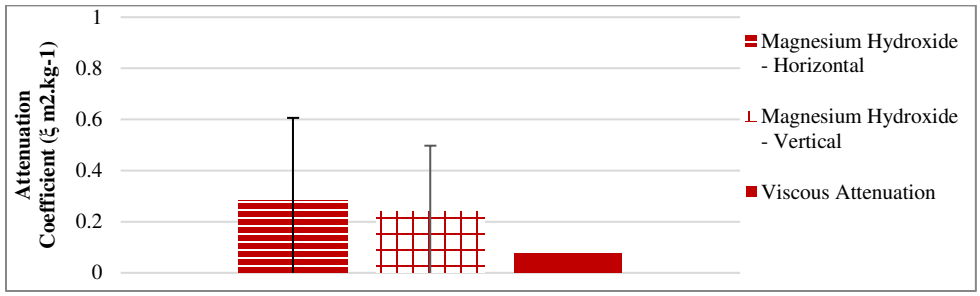

Fig. 12. Viscous attenuation coefficients for suspensions of magnesium hydroxide

Interestingly also, the attenuation coefficients from calcite suspensions are higher than the coefficients from the magnesium hydroxide suspensions, which would be expected from changes in viscous absorption, due to the larger size of the magnesium hydroxide. The effect of viscous absorption was probed further by comparing the measured attenuation coefficients to estimations from Urick's theory (Eqs. (11)-(12)). While the theoretical estimates for calcite are also above those of magnesium hydroxide, as expected, both calculated values make-up a great portion of the measured attenuation coefficients, most significantly for the calcite system. It is thought the main reason for the discrepancy is that both calcite and magnesium hydroxide systems can undergo natural aggregation, due to their low surface charges. It may be that shear conditions within the pipe loop are lower than in the Mastersizer test cell, and thus actual representative sizes within the pipe system are larger than estimated by laser diffraction. It is also noted that the calculated values are based on a single mean diameter value, while it was evident from size measurements that both suspensions had relatively broad distributions.

CONCLUSIONS

- An increase in concentration within the pipe leads to increased attenuation across the pipe.
- The addition of magnesium hydroxide and calcite into the suspension decreases the speed of sound below the speed of sound in water.
- Magnesium hydroxide produced more accurate attenuation profiles with less variation and closer predictions to linear correlations.
- The vertical pipe arrangement was more efficient and accurate, producing a stronger signal strength and closer sedimentation attenuation coefficients to the calibration data.
- The horizontal pipe arrangement was more prone to particle segregation which led to noisy profiles in the first half of the pipe.
- Calcite attenuates the signal more due to the presence of fines which increases the viscous attenuation.

- Attenuation coefficient values for magnesium hydroxide are more sensitive to scattering losses in comparison to calcite, this is due to the increased particle size and presence of aggregates.
- The particle size for both calcite and magnesium hydroxide are very small, this means that the level of backscatter is low. A lower backscatter level produces a noisy profile as the UVP is trying to analyse the small component of scatter.

ACKNOWLEDGEMENT

The authors thank the Engineering and Physical Sciences Research Council (EPSRC) UK and Sellafield Ltd for funding through the Next Generation Nuclear (NGN) Centre for Doctoral Training (EP/L015390/1).

REFERENCES

1. Biggs, S., Fairweather, M., Hunter, T., Omokanye, Q., and Peakall, J. Engineering Properties of Nuclear Waste Slurries. In: *International Conference on Radioactive Waste Management and Environmental Remediation*, *11-15 October 2009, Liverpool.* Liverpool: ASME, 2009; doi: 10.1115/ICEM2009-16378

2. Adams, J.F.W., Biggs, S.R., Fairweather, M., Yao, J. and Young, J. Transport of Nuclear Waste Flows: A Modelling and Simulation Approach. In: *ASME 14th Conference on Environmental Remediation and Radioactive Waste Management, January 2011, France.* France: ASME, 2011; doi: 10.1115/ICEM2011-59136

3. Gregson, C.R., Goddard, D.T., Sarsfield, M.J. and Taylor, R.J. Combined electron microscopy and vibrational spectroscopy study of corroded Magnox sludge from a legacy spent nuclear fuel storage pond. *Journal of Nuclear Materials.* 2011, **412**(1), doi: 10.1016/j.jnucmat.2011.02.046

4. Takeda. Y. ed. Ultrasonic Doppler Velocity Profiler for Fluid Flow. New York: Springer Publishing, 2012.

5. Hussain, S.T., Hunter, T.N., Peakall, J. and Barnes, M. Utilisation of underwater acoustic backscatter systems to characterise nuclear waste suspensions remotely. *Proceedings of Meetings on Acoustics*. 2020, **40**, 070005; doi: 10.1121/2.0001303.

6. Sassi, M.G., Hoitink, A.J.F. and Vermeulen, B. Impact of sound attenuation by suspended sediment on ADCP backscatter calibrations. *Water Resources Research.* 2012, **48**(9); doi: 10.1029/2012WR012008

7. MET-FLOW. *Products/ Profilers*. [Online]. 2021. [Accessed 16 April 2021]. Available at: https://met-flow.com/technology/products/uvp-duo-profilers/

8. Hriljac, J, Boxall, C, Currell, F et al. (2018) The DISTINCTIVE University Consortium Theme 3: Legacy Ponds and Silo Wastes. In: *Proceedings of the 44th Annual Waste Management Conference. WM2018: 44th Annual Waste Management Conference, 18-22 Mar 2018*, *Phoenix, AZ, USA*. USA: Waste Management Symposia, pp. 6180-6194. ISBN 978-1-5108-6764-2

9. Hussain, S.T., Peakall, J., Barnes, M., and Hunter, T. Characterising Flocculated Suspensions with an Ultrasonic Velocity Profiler (UVP) in Backscatter Mode. In: *IEEE IUS 2021, September 2021, Virtual.* China: IEEE, 2021.

10. Hunter, T., Biggs, S., Young, J., Fairweather, M., and Peakall, J. Ultrasonic Techniques for the In Situ Characterization of Nuclear Waste Sludges. In: *WM2011 Conference, February 27 – March 3, Phoenix, AZ, USA.* USA: Waste management symposia, pp. 1-12; doi: 10.1115/ICEM2011-59111

11. Rice, H. P. et al., 2015. Measurement of particle concentration in horizontal, multiphase pipe flow using acoustic methods: Limiting concentration and the effect of attenuation. *Chemical Engineering Science*, 126(January 2015), pp. 745-758.

12. Downing, A., Thorne, P. D. and Vincent, C. E. Backscattering from a suspension in the near field of a piston transducer. *Journal of the Acoustical Society of America*. 1995, **97**(3), pp. 1614-1620; doi: 10.1121/1.412100

13. Han, E., Ha, N.V., and Jaeger, H.M., 2017. Measuring the porosity and compressibility of liquid-suspended porous particles using ultrasound. *Soft Matter*, **13**(1), pp. 3506-3513; doi: 10.1039/C7SM00182G.

14. Urick, R. J., 1948. The Absorption of Sound in Suspensions of Irregular Particles. *The Journal of the Acoustical Society of America,* 20(3), pp. 283-289.

15. Tanaka, M., Girard, G., Davis, R., Peuto, A. and Bignell, N. Recommended table for the density of water between 0°C and 40°C based on recent experimental reports. *Metrologia.* 2001, **38**(4).

16. Carmichael, R.S. *Practical Handbook of Physical Properties of Rocks and Minerals.* Oxfordshire: Taylor and Francis, 1988.

17. Hermann, A., and Mookherjee, M. High-pressure phase of brucite stable at Earth's mantle transition zone and lower mantle conditions. *PNAS.* 2016. **113**(49), pp. 13971-13976; doi: 10.1073/pnas.1611571113.

18. Betteridge, K. F., Thorne, P. D. and Cooke, R. D. Calibrating multi-frequency acoustic backscatter systems for studying near-bed suspended sediment transport processes. *Continental Shelf Research*. 2008, **28**(2), pp. 227-235; doi: 10.1016/j.csr.2007.07.007

19. Martin Marietta. 2021. Versamag 30. [Online]. [Accessed 10 November 2021]. Available from: Versamag - MH | Martin Marietta Magnesia Specialties, LLC

20. Omya North America. *AZ Calcium Carbonate. Omya.* [Online]. [Accessed 10 November 2021]. Available from: OMYACARB® Technical Data Sheets (matweb.com)

21. Bux, J. & Peakall, J. B. S., 2015. In situ characterisation of a concentrated colloidal titanium dioxide settling suspension and associated bed development: Application of an acoustic backscatter system. *Powder Technology*, 284(1), pp. 530-540.

22. Lockwood, A.P.G., Shun, P.K., Peakall, J., Warren, N.J., Barber, T., Basharat, N., Randall, G., Barnes, M., Harbottle, D., and Hunter, T.N., 2021. Flotation using sodium dodecyl sulphate and sodium lauroyl isethionate for rapid dewatering of $Mg(OH)_2$ radwaste suspensions. *RSC Adv,* **11**(1), pp. 18661-18675; doi: 10.1039/D1RA01222C. lockwood vm micrograph

23. Biron, M. *Thermoplastics and Thermoplastic Composites*. Oxford: Elsevier, 2007.

24. Nguyen, T.H.L., and Park, S. Multi-Angle Liquid Flow Measurement Using Ultrasonic Linear Array Transducer. *Sensors.* 2020, **20**(2); doi: 10.3390/s20020388**.**

25. Johnson, B.L., Holland, M.R., Miller, J.G., and Katz, J.I. *Ultrasonic Attenuation and Speed of Sound of Cornstarch Suspensions.* Washington: Washington University, 2012.

26. Denny, M. *Air and Water.* Princeton: Princeton University. 1993.

27. Hunter, T.N., Peakall, J., and Biggs, S. An acoustic backscatter system for in situ concentration profiling of settling flocculated dispersions. *Minerals Engineering.* 2012, 12(3), pp. 20-27; doi: 10.1016/j.mineng.2011.12.003

28. Kotze, R., Adler, A., Sutherland, A., and Deba, C.N. Evaluation of Electrical Resistance Tomography imaging algorithms to monitor settling slurry pipe flow. *Flow Measurement and Instrumentation.* 2019, 68(**1**), 101572; doi: 10.1016/j.flowmeasinst.2019.101572

29. Holmer, C.I., and Heymann, F.J. Transmission of sound through pipe walls in the presence of flow. *Journal of Sound and Vibration.* 1980. **70**(2), pp. 275-301; doi: 10.1016/0022-460X(80)90601-X

30. Rice, H. P. Transport, and deposition behaviour of model slurries in closed pipe flow Intellectual property and publication statements. Ph.D. thesis, University of Leeds, 2013.

31. Guyson Ltd. Glass Blast Media. [Online]. [Accessed June 13, 2020]. Available from: https://s3-eu-west-1.amazonaws.com/resources.guyson.co.uk/product-downloads/Honite.pdf?mtime=20200117140801.